\



High-efficiency asymmetric diffraction based on PT-antisymmetry in quantum dot molecules

Guangling Cheng(程广玲), Yongsheng Hu(胡永升), Wenxue Zhong(钟文学), and Aixi Chen(陈爱喜)
Citation: Chin. Phys. B, 2022, 31 (**1**): 014202. DOI: 10.1088/1674-1056/ac0422
Journal homepage: http://cpb.iphy.ac.cn; http://iopscience.iop.org/cpb

What follows is a list of articles you may be interested in

Lattice plasmon mode excitation via near-field coupling

Yun Lin(林蕴), Shuo Shen(申烁), Xiang Gao(高祥), and Liancheng Wang(汪炼成)
Chin. Phys. B, 2022, 31 (**1**): 014214. DOI: 10.1088/1674-1056/ac0523

High-resolution three-dimensional atomic microscopy via double electromagnetically induced transparency

Abdul Wahab
Chin. Phys. B, 2021, 30 (**9**): 094202. DOI: 10.1088/1674-1056/abf0fd

Quantum storage of single photons with unknown arrival time and pulse shapes

Yu You(由玉), Gong-Wei Lin(林功伟), Ling-Juan Feng(封玲娟), Yue-Ping Niu(钮月萍), and Shang-Qing Gong(龚尚庆)
Chin. Phys. B, 2021, 30 (**8**): 084207. DOI: 10.1088/1674-1056/abfbd3

Monte Carlo simulations of electromagnetically induced transparency in a square lattice of Rydberg atoms

Shang-Yu Zhai(翟尚宇) and Jin-Hui Wu(吴金辉)
Chin. Phys. B, 2021, 30 (**7**): 074206. DOI: 10.1088/1674-1056/abd75a

Optimization of terahertz monolithic integrated frequency multiplier based on trap-assisted physics model of THz Schottky barrier varactor

Lu-Wei Qi(祁路伟), Jin Meng(孟进), Xiao-Yu Liu(刘晓宇), Yi Weng(翁祎), Zhi-Cheng Liu(刘志成), De-Hai Zhang(张德海)†, Jing-Tao Zhou(周静涛)‡, and Zhi Jin(金智)
Chin. Phys. B, 2020, 29 (**10**): 104212. DOI: 10.1088/1674-1056/abab74

High-efficiency asymmetric diffraction based on PT-antisymmetry in quantum dot molecules

Guangling Cheng(程广玲)[1], Yongsheng Hu(胡永升)[1], Wenxue Zhong(钟文学)[1], and Aixi Chen(陈爱喜)[2,†]

[1] *Department of Applied Physics, East China Jiaotong University, Nanchang* 330013, *China*
[2] *Department of Physics, Zhejiang Sci-Tech University, Hangzhou* 310018, *China*

(Received 28 April 2021; revised manuscript received 18 May 2021; accepted manuscript online 24 May 2021)

We present preparation of asymmetric grating with higher diffraction efficiency in quantum dot molecules by combining the tunneling effect and parity-time antisymmetry. In the presence of tunneling between two quantum dots, the system exhibits the striking PT antisymmetry via spatially modulating the driving field and the detuning with respect to the driven transition. For this reason, the asymmetric grating could be achieved. The results show that the diffraction efficiency can be adjustable via changing the driving intensity, detuning, tunneling strength, and interaction length, and then the high-order diffraction can be reached. The scheme provides a feasible way to obtain the direction-controlled diffraction grating, which can be helpful for optical information processing and realization of controllable optical self-image.

Keywords: asymmetric diffraction grating, PT antisymmetry, tunneling effect

PACS: 42.50.Gy, 32.80.Qk **DOI:** 10.1088/1674-1056/ac0422

1. Introduction

As an optical element with periodic structure, the grating can diffract the incident light beam to a high-order diffraction direction, which has important applications in the field of industrial production and has also been widely concerned by researchers in the quantum field.[1] By replacing the traveling-wave field with the standing-wave field in an electromagnetically induced transparency (EIT) system,[2,3] in which the absorption and dispersion become spatially periodic, electromagnetically induced grating (EIG) has been presented[4–6] and could provide the potential applications in quantum optics and laser physics.[7–9] For the probe resonance in the EIT medium, the dispersion is negligibly small with the transparency window and the medium acts as an amplitude grating, which leads to low-efficiency diffraction in the high-order direction. While the probe detuning appears, the dispersion will be enlarged with the small absorption and the grating could be formed. To improve the high-order diffraction intensities, the schemes for phase grating have been presented in different systems.[10–15]

Recently, the optical systems provide a versatile platform for the study of non-Hermitian physics with respect to parity-time (PT) symmetry and PT antisymmetry.[16–23] In particular, coherently prepared multilevel atoms may open up new opportunities for manipulating light in non-Hermitian optics, due to their easy reconfiguration, flexible tunability, actively control techniques, and enhanced nonlinear effects. Based on spatially modulating the refractive index with gain and absorption, the optical PT symmetry with $n(x) = n^*(-x)$ in the given direction has been theoretically and experimentally investigated in laser-driven multi-level atomic gases.[24–26] It is found that PT symmetry could be used to generate asymmetric diffraction grating.[27–30] As the counterpart of conventional PT symmetry, PT antisymmetry satisfying $n(x) = -n^*(-x)$ has been investigated in the driven atomic systems,[26,31–34] which does not require optical gain and relaxes the condition of the interplay of gain and loss. PT antisymmetry has motivated various practical applications including unidirectional reflectionless,[31] constant refraction,[35] Hermitian scattering,[36] and coherent switch.[37] Most recently, PT antisymmetry is applied to explore asymmetric diffraction gratings in the Rydberg system[38] and atomic lattices.[39]

In parallel, semiconductor quantum dots have attracted a great deal of attention due to their distinct features[40–42] and are widely used in quantum optics to realize many interesting phenomena such as electromagnetically induced transparency,[43] four-wave mixing,[44] transfer of optical vortices,[45] and resonance fluorescence.[46] Importantly, the system of quantum dot molecules (QDM) formed via tunneling effect in two or more quantum dots has been brought into focus in recent years,[47–51] in which electrons can tunnel through the potential barrier between quantum dots. The tunneling effects between quantum dots play an important role in inducing coherent quantum phenomena such as slow light,[52] Kondo-peak splitting,[53] tunneling induced absorption,[54] tunneling-induced transparency,[55] and manipulation and exchange of light.[56]

Here, we investigate the properties of asymmetric light diffraction via the optical PT antisymmetry in the QDM system with the four-level structure, where the tunneling occurs

†Corresponding author. E-mail: aixichen@zstu.edu.cn

© 2022 Chinese Physical Society and IOP Publishing Ltd

between two quantum dots. Based on the spatial modulations of the driving field and driving detuning, the symmetric absorption and antisymmetric dispersion in the space are existent, which lead to the presence of PT antisymmetry. The results show that the asymmetric grating with high intensities in both the first-order and high-order directions are obtained via properly choosing the system parameters. Furthermore, the diffraction direction among the negative or positive orders can be controlled by changing the sign of the modulating detuning. Our scheme may be served as powerful building blocks for developing novel photonic devices and implementing the information processing.

2. Model and equation

We consider a system of asymmetric double quantum dots, where two individual quantum dots are coupled by tunneling. Such a system can be treated as a four-level system and it is shown in Fig. 1(a). A weak traveling-wave probe field $E_{\rm p}$ with frequency $\omega_{\rm p}$ probes the transition of ground state $|1\rangle$ to excited state $|2\rangle$, and a standing-wave driving field $E_{\rm c}$ with frequency $\omega_{\rm c}$ acts on excited state $|3\rangle$ and excited state $|4\rangle$. The tunneling of two quantum dots exists between the transition $|2\rangle \leftrightarrow |3\rangle$. The Rabi frequency of the probe and driving fields are $\Omega_{\rm p} = \boldsymbol{\mu}_{12}\cdot\boldsymbol{E}_{\rm p}/\hbar$ and $\Omega_{\rm c} = \Omega_0 \sin(\pi x/\Lambda)$ with $\Omega_0 = \boldsymbol{\mu}_{34}\cdot\boldsymbol{E}_{\rm c}/\hbar$, respectively, where $\boldsymbol{\mu}_{ij}$ is the associated dipole transition matrix element from state $|i\rangle$ to $|j\rangle$ and Λ is the spatial period of the standing-wave driving field. Then, the Hamiltonian in the rotating frame and under the rotating-wave approximations is given by ($\hbar = 1$)

$$\begin{aligned} H_{\rm I} =\ & \Delta_{\rm p}\sigma_{22} + \left(\Delta_{\rm p}+\omega_{32}\right)\sigma_{33} + \left(\Delta_{\rm p}+\omega_{32}+\Delta_{\rm c}\right)\sigma_{44} \\ & -\left(\Omega_{\rm p}\sigma_{21} + T_{\rm e}\sigma_{23} + \Omega_{\rm c}\sigma_{43} + {\rm H.c.}\right), \end{aligned} \tag{1}$$

where $\Delta_{\rm p} = \omega_{21} - \omega_{\rm p}$ is the detuning of the probe field, and $\Delta_{\rm c} = \omega_{43} - \omega_{\rm c}$ is the detuning of the driving field; ω_{ij} is the transition frequency between levels $|i\rangle \leftrightarrow |j\rangle$. $T_{\rm e}$ is the tunneling coupling strength between the transition $|3\rangle \leftrightarrow |2\rangle$.

The dynamics of the QDM system can be described by a master equation of the density operator

$$\frac{\partial\rho}{\partial t} = -{\rm i}[H,\rho] + \mathscr{L}\rho, \tag{2}$$

where $\mathscr{L}\rho$ describes the dissipation of the system. Combining Eqs. (1) and (2), it is straightforward to further obtain the following density matrix equations:

$$\dot{\rho}_{21} = {\rm i}\Omega_{\rm p}\left(\rho_{11}-\rho_{22}\right) - {\rm i}\left(\Delta_{\rm p} - {\rm i}\gamma_2\right)\rho_{21} + {\rm i}T_{\rm e}\rho_{31}, \tag{3}$$

$$\dot{\rho}_{31} = {\rm i}T_{\rm e}\rho_{21} - {\rm i}\Omega_{\rm p}\rho_{32} - {\rm i}\left(\Delta_{\rm p}+\omega_{32}-{\rm i}\gamma_3\right)\rho_{31} + {\rm i}\Omega_{\rm c}\rho_{41}, \tag{4}$$

$$\dot{\rho}_{41} = -{\rm i}\Omega_{\rm p}\rho_{42} + {\rm i}\Omega_{\rm c}\rho_{31} - {\rm i}\left(\Delta_{\rm c}+\Delta_{\rm p}+\omega_{32}-{\rm i}\gamma_4\right)\rho_{41}, \tag{5}$$

with γ_i being the total quantum dissipation of the energy-level $|i\rangle$ including decay rate and dephasing rate. Under the condition of a weak probe field $\Omega_{\rm p} \ll \Omega_{\rm c}, T_{\rm e}$ and the initial condition of $\rho_{11}(0) = 1$ and $\rho_{22}(0) = \rho_{32}(0) = \rho_{42}(0) = 0$, we solve the above equations and obtain the steady-state solution

$$\rho_{21} = \frac{\Omega_{\rm p}\left(\Upsilon_3\Upsilon_4 - \Omega_{\rm c}^2\right)}{\Upsilon_2\Upsilon_3\Upsilon_4 - \Upsilon_2\Omega_{\rm c}^2 - \Upsilon_4 T_{\rm e}^2}, \tag{6}$$

where $\Upsilon_2 = \Delta_{\rm p} - {\rm i}\gamma_2$, $\Upsilon_3 = \Delta_{\rm p} + \omega_{32} - {\rm i}\gamma_3$ and $\Upsilon_4 = \Delta_{\rm c} + \Delta_{\rm p} + \omega_{32} - {\rm i}\gamma_4$. We know that the polarization of the present system is determined by $P_{\rm p} = N\mu_{12}\rho_{21} = \varepsilon_0\chi_{\rm p}E_{\rm p}$, where $N = \Gamma/V$ is the electronic number density, V is the volume of a single quantum dot. Then we can obtain the susceptibility of the four-level system to the probe field

$$\chi_{\rm p} = \frac{\Gamma|\mu_{12}|^2}{V\varepsilon_0\hbar}\frac{\rho_{21}}{\Omega_{\rm p}}, \tag{7}$$

with $\chi_{\rm p} = \chi_{\rm p}^{\rm R} + {\rm i}\chi_{\rm p}^{\rm I}$. The real part $\chi_{\rm p}^{\rm R}$ and the imaginary part $\chi_{\rm p}^{\rm I}$ describe the dispersion properties and the absorption properties of the system, respectively. In our analysis, the realistic experimental parameters for InAs self-assembled QDMs are under consideration.[57] $\Gamma = 6\times10^{-3}$ is the optical confinement factor, and the QDM surface density is 2×10^{11} cm^{-2}.

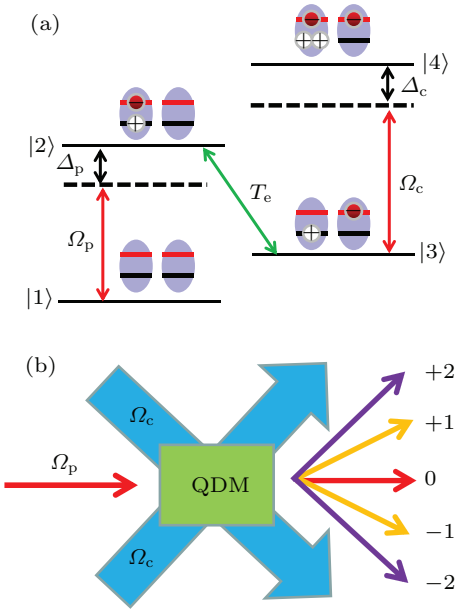


Fig. 1. (a) Diagram of the four-level QDM system with a probe field and a driving field. The electron and hole are shown by ⊖ and ⊕, respectively. (b) Schematic propagations of driving field and probe field.

In the slow amplitude approximation and the steady-state regime, the dynamic response of the probe field can be described by Maxwell's equation

$$\frac{\partial E_{\rm p}}{\partial z} = \frac{{\rm i}\pi}{\lambda_{\rm p}}\left(\chi_{\rm p}^{\rm R} + {\rm i}\chi_{\rm p}^{\rm I}\right)E_{\rm p}, \tag{8}$$

with $\lambda_{\rm p}$ being the wavelength of the probe field. Therefore, the transmission function of the probe field with interaction length L is derived as

$$T(x) = {\rm e}^{-\chi_{\rm p}^{\rm I}L/z_0}\,{\rm e}^{{\rm i}\chi_{\rm p}^{\rm R}L/z_0}, \tag{9}$$

where $z_0 = V\varepsilon_0\hbar\lambda_p/(\pi\Gamma|\mu_{12}|^2)$ is treated as an unit for L. The first term $e^{-\chi_p^I L/z_0}$ and the second part $e^{i\chi_p^R L/z_0}$ represent the amplitude and phase component, respectively. By solving the Fourier transform of $T(x)$, we can obtain the diffraction intensity of probe field, which is given by

$$I_p(\theta_n) = |E(\theta_n)|^2 \frac{\sin^2(M\pi\Lambda\sin\theta_n/\lambda_p)}{M^2\sin^2(\pi\Lambda\sin\theta_n/\lambda_p)}, \tag{10}$$

with the intensity in a single period as

$$E(\theta_n) = \int_0^1 dx T(x)\exp(-i2\pi x\Lambda\sin\theta_n/\lambda_p). \tag{11}$$

Here, $n = \Lambda\sin\theta_n/\lambda_p$ is the diffraction order; θ_n denotes the n-order diffraction angle of x-axis with respect to the z-direction, and M stands for the number of space period in x-axis.

To realize PT antisymmetry and the lopsided and controllable higher-efficiency diffraction, the periodically spatial modulation to driving detuning $\Delta_c(x)$ is rewritten as

$$\Delta_c(x) = \Delta_{c0} + \delta\Delta_c\sin(2\pi x/\Lambda), \tag{12}$$

where Δ_{c0} is the constant detuning and $\delta\Delta_c$ describes the modulation amplitude of detuning. As shown previously,[28] the extra spatially modulated lasers are applied to induce the AC Stark effect, which could realize a periodic change of energy shift of state $|4\rangle$. It is expected that the combination of periodic modulation of Ω_c and Δ_c can realize PT antisymmetry in the quantum dot system, where the symmetric absorption and antisymmetric dispersion, i.e., $\chi_p(x) = -\chi_p^*(-x)$, and the complex refractive index with $n(x) = -n^*(-x)$ via the relation $n \approx 1 + \chi_p/2$ are reached and the interesting results will be achieved.

3. Result and discussion

In the following, all physical parameters are measured in terms of decay rates γ_2 and the actual experimental parameters of InAs self-assembled QDMs are selected with $\gamma_2 = \gamma_4 = 10^3\gamma_3 = 10$ μeV.[58] We first discuss the influence of driving detuning Δ_c on the distribution of the system susceptibility χ_p, transmission $|T(x)|$ and diffraction intensity $I_p(\theta)$ in Fig. 2, where the corresponding parameters are given by $\Delta_p = 0$, $T_e = 2$, $\Omega_0 = 4$, $\gamma_2 = \gamma_4 = 1 = 10^3\gamma_3$, $L = 20z_0$, $M = 10$, $\Lambda/\lambda_p = 4$, (a1)–(a3) $\Delta_{c0} = 20$, $\delta\Delta_c = 0$ and (b1)–(b3) $\Delta_{c0} = 0$, $\delta\Delta_c = 20$. When the detuning of the driving field consists only of constant detuning $\Delta_{c0} = 20$, $\delta\Delta_c = 0$, as shown in Figs. 2(a1)–2(a3), we can see that absorption (red-dashed) and dispersion (blue-solid) are even functions of coordinate x. As is expected, the probe field is diffracted symmetrically in both positive and negative directions and high efficiency at first-order diffraction. Differently, it is clear from Figs. 2(b1)–2(b3) that the absorption is a symmetric function, but the dispersion becomes an antisymmetric function when $\Delta_{c0} = 0$, $\delta\Delta_c = 20$. The PT antisymmetric region is formed due to the mutual modulations between driving detuning and standing-wave driving fields. In this region, transmission and diffraction shown in Fig. 2(b) greatly change compared with Fig. 2(a) and lead to the formation of asymmetric diffraction which only contains positive angles. It is obvious that QDM can successfully diffract a probe beam only in the positive direction under the action of PT antisymmetry. Compared with Figs. 2(a3) and 2(b3), we can see that the first-order diffraction of the classical symmetric grating can reach 0.168. However, under the condition of the same parameters, the asymmetric grating can reach 0.26, and the second-order diffraction can reach 0.164. Therefore, the grating with an asymmetric diffraction pattern could be achieved by introducing the modulation of driving detuning and meanwhile the diffraction efficiency is greatly improved.

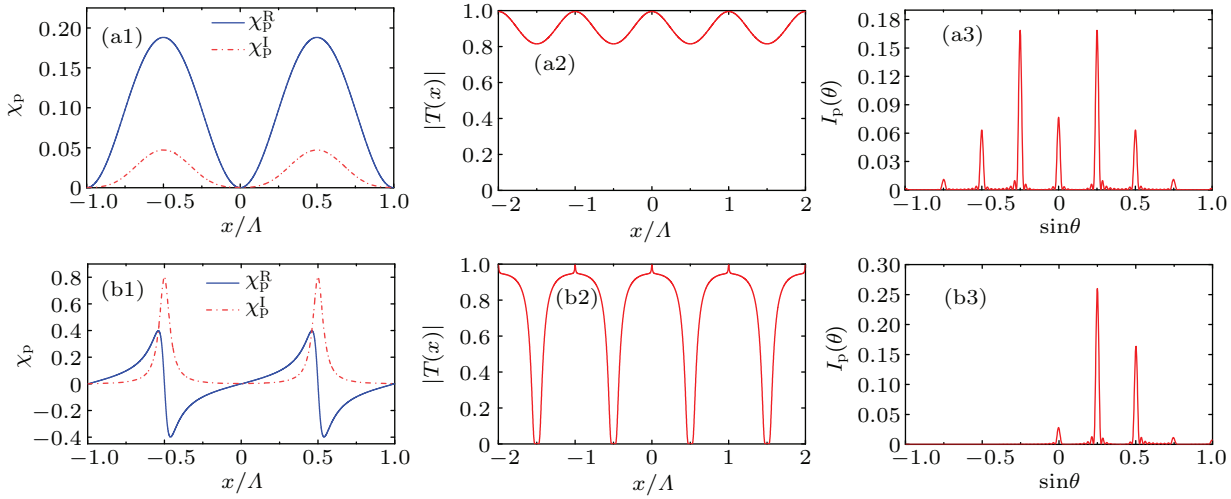


Fig. 2. Absorption χ_p^I and dispersion χ_p^R, transmission $|T(x)|$ and diffraction patterns $I_p(\theta)$. The corresponding parameters are given by $\Delta_p = 0$, $T_e = 2$, $\Omega_0 = 4$, $\gamma_2 = \gamma_4 = 1 = 10^3\gamma_3$, $L = 20z_0$, $M = 10$, $\Lambda/\lambda_p = 4$, (a1)–(a3) $\Delta_{c0} = 20$, $\delta\Delta_c = 0$ and (b1)–(b3) $\Delta_{c0} = 0$, $\delta\Delta_c = 20$.

Next, we focus on the influence of tunneling strength T_e and Rabi frequency Ω_0 on diffraction intensity. The Fraunhofer diffraction patterns versus $\sin\theta$ for the different parameters are illustrated in Fig. 3 with $L = 25z_0$, $\Delta_{c0} = 0$, $\delta\Delta_c = 25$, and the other parameters as same as those in Fig. 2. As can be seen from Fig. 3(a), for the small tunneling intensity with $T_e = 1$, the diffraction of the probe field appears in the third-order direction, and its diffraction intensity can reach 0.134. Increasing tunneling strength to $T_e = 1.3$ and $T_e = 2$, the diffraction intensities in second-order and first-order diffraction peaks are 0.24 and 0.45, respectively. For the large tunneling strength of $T_e = 3.3$, the diffraction gradually tends to the center, and the intensity of higher-order diffraction is very small. The reason for this phenomenon is that the dispersion of the medium to the probe field decreases with the increase of tunneling intensity, which makes the diffraction tends to the zero-order direction. In contrast, when the Rabi frequency is small, the energy is concentrated in the central diffraction at $\Omega_0 = 1.3$ [see Fig. 3(b)]. As the Ω_0 continues to increase to 2, 3.5, and 4.6, the diffraction intensity gradually approaches the higher-order direction with values of 0.45, 0.24, and 0.139, corresponding to first-order, second-order, and third-order diffraction, respectively.

Now we check into the effects of the modulation amplitude $\delta\Delta_c$ of driving detuning and Rabi frequency Ω_0 on the diffraction intensity of the asymmetric diffraction grating. The intensity of the diffraction peak $I_p(\theta_n)$ $(n = 1,2,3)$ in Fig. 4 is based on the positive direction diffraction. We first analyze the first-order diffraction in Fig. 4(a). It is obvious that the first-order diffraction intensity has a high value near the $\Omega_0 = 3$, and increases with the modulation amplitude $\delta\Delta_c$. At $\Omega_0 = 3.1$, $\delta\Delta_c = 30$, the diffraction intensity can reach the maximum value 0.462, and the second-order and third-order diffraction intensity is close to 0, which indicates that the energy of the probe field is well concentrated in the first-order direction. As Ω_0 continues to increase, the first-order diffraction intensity gradually decreases to 0 and is not changing at the end. Second-order and third-order diffraction exhibit similar variations to the first-order diffraction, as shown in Figs. 4(b) and 4(c). The difference is that the second-order diffraction is accompanied by a less intense diffraction region, and the third-order has two regions. This is because the diffraction peak is very sensitive to the value of $\delta\Delta_c$ and Ω_0, and with the increase of Ω_0, the dispersion of the medium to the probe field increases gradually, which causes the diffraction intensity to shift to the higher-order direction so that the diffraction peaks exhibit similar oscillatory behavior. In addition, by controlling $\delta\Delta_c$ and Ω_0, we can obtain high-order diffraction with high efficiency, in which second-order diffraction can reach 0.249 and even the third-order diffraction can achieve a diffraction intensity as high as 0.145.

As an asymmetric diffraction grating, it is vital to know how to control its diffraction direction. Thus, last but not least, we discuss the factors that influence the diffraction

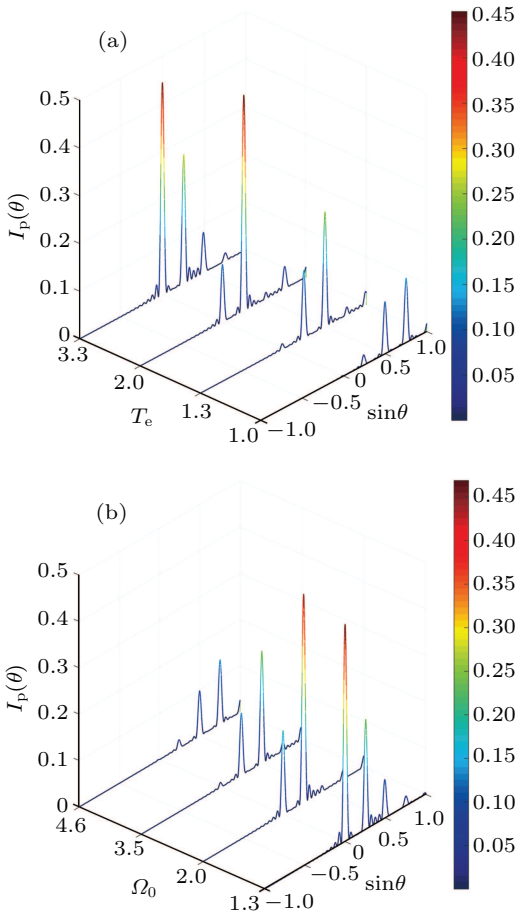


Fig. 3. The diffraction intensity $I_p(\theta)$ versus the coordinate $\sin\theta$ at different T_e and Ω_0 with $L = 25z_0$, $\Delta_{c0} = 0$, $\delta\Delta_c = 25$, (a) $\Omega_0 = 3$, (b) $T_e = 1.5$, and the other parameters as same as those in Fig. 2.

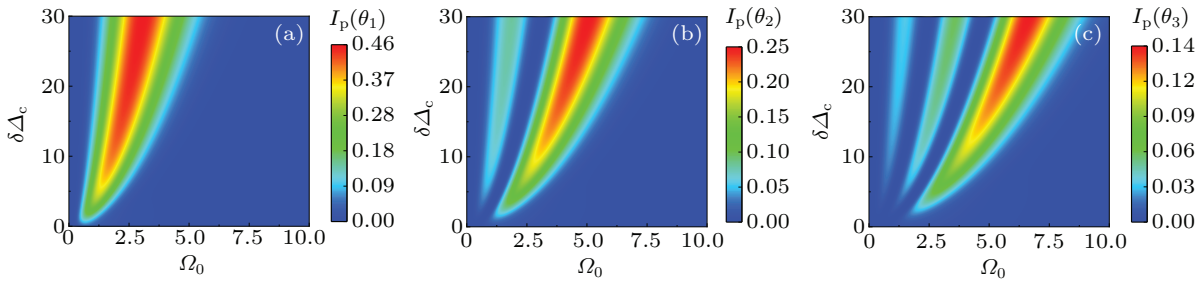


Fig. 4. The peak diffraction intensity $I_p(\theta_n)$ depending on the modulation amplitude $\delta\Delta_c$ and Rabi frequency Ω_0, where the parameters are $T_e = 2$, $L = 25z_0$, $\Delta_{c0} = 0$ and the rest parameters are same as those in Fig. 2.

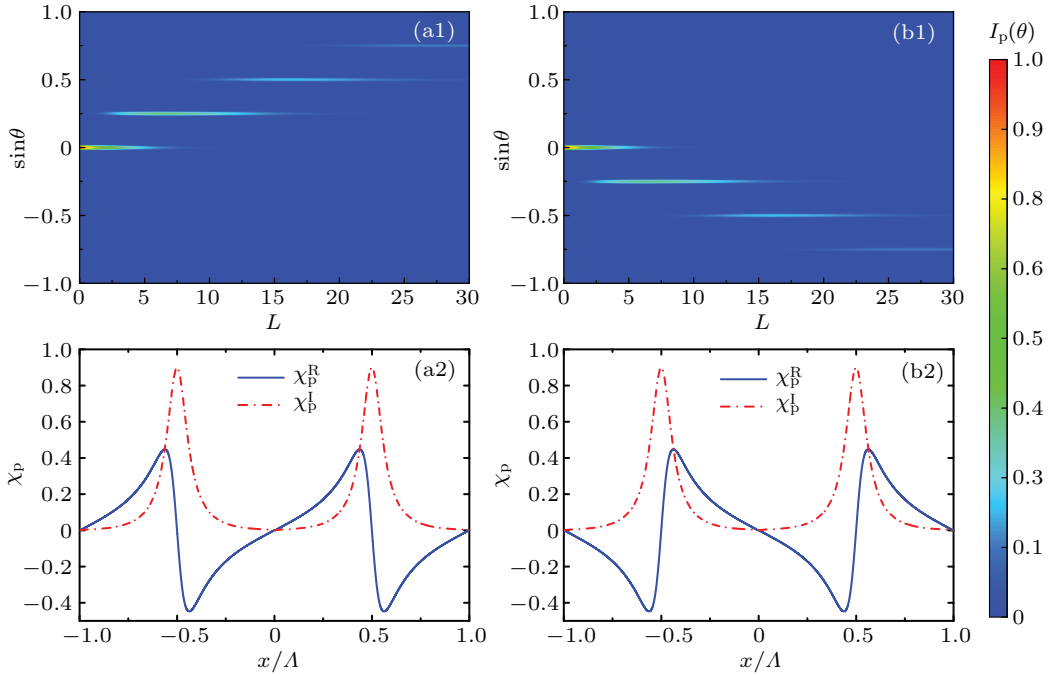


Fig. 5. The diffraction intensity $I_{\rm p}(\theta)$ as a function of $\sin\theta$ and L with $\Delta_{\rm c0}=0$, [(a1), (a2)] $\delta\Delta_{\rm c}=25$, [(b1), (b2)] $\delta\Delta_{\rm c}=-25$, where the other parameters are the same as those in Fig. 2.

direction of the asymmetric diffraction grating. Figures 5(a1) and 5(b1) show that the diffraction intensity changes with the interaction length L and $\sin\theta$. It is shown in Fig. 5(a1) that a diffraction pattern only has positive angle diffraction, which is realized by the modulation of absorption and dispersion relations in Fig. 5(a2) ($\delta\Delta_{\rm c}=25$). On the contrary, Fig. 5(b1) shows the diffraction pattern with negative angles, which is formed by the absorption and dispersion coefficients modulated in Fig. 5(b2) ($\delta\Delta_{\rm c}=-25$). For the present QDM system without gain, the positive and negative amplitude modulation of the detuning cannot change the symmetry of absorption modulation. Fortunately, by comparing to Figs. 5(a2) and 5(b2), we can see that the change of the modulation amplitude of the driving detuning causes the switch of the positive and negative relation of the dispersion, which changes the direction of the diffraction from the positive angle to the negative angle. It is obvious that the diffraction direction of an asymmetric grating based on PT antisymmetry is mainly dependent on the spatial relation of the dispersion symbol, and it can be easily manipulated by simply changing the symbol of the modulation amplitude of the driving detuning. On the other hand, it can be seen from Figs. 5(a1) and 5(b1) that, with the increase of the interaction length L, the diffraction intensity moves towards the higher-order direction due to the increasing phase modulation.

4. Conclusion

In conclusion, the asymmetric diffraction grating with higher diffraction efficiency is studied in the system of double quantum dots. Combining the tunneling effect between two quantum dots and the spatial modulations of the driving field and driving detuning, the system exhibits the complex refractive index with $n(x)=-n^*(-x)$. Then, the optical PT antisymmetry appears in such a system, which is responsible for the preparation of lopsided diffraction grating. It is obvious that the diffraction intensity in high-order direction exceeds that of the traditional symmetric grating and can be easily adjusted by changing the driving strength, detuning, tunneling strength, and interaction length. Our research provides a feasible scheme for greatly improving diffraction efficiency and effectively controlling diffraction direction, which is conducive to various applications of quantum information processing and optical transmissions.

Acknowledgements

This work is supported by the National Natural Science Foundation of China (Grant Nos. 11905064, 11775190 and 11565013) and the Scientific Research Foundation of Jiangxi Provincial Education Department, China (Grant No. GJJ200624).

References

[1] Palmer C and Loewen E 2005 *Diffraction Grating Handbook* (New York: Newport Corp, Rochester)
[2] Harris S E 1997 *Phys. Today* **50** 36
[3] Wang D, Wu J Z and Zhang J X 2016 *Chin. Phys. B* **25** 064202
[4] Ling H Y, Li Y Q and Xiao M 1998 *Phys. Rev. A* **57** 1338
[5] Yuan J P, Wu C H, Li Y H, Wang L R, Zhang Y, Xiao L T and Jia S T 2019 *Front. Phys.* **14** 52603
[6] Dong Y B, Li J Y and Zhou Z Y 2017 *Chin. Phys. B* **26** 014202
[7] Bajcsy M, Zibrov A S and Lukin M D 2003 *Nature* **426** 638
[8] Ru J M, Wu Z K, Zhang Y G, Wen Fe and Gu Y Z 2020 *Front. Phys.* **15** 52503

[9] Brown A W and Xiao M 2005 *Opt. Lett.* **30** 699
[10] Araujo L E E 2010 *Opt. Lett.* **35** 977
[11] Hu Y S, Cheng G L and Chen A X 2020 *Opt. Express* **28** 29805
[12] Wan R G, Kou J, Jiang L and Gao J Y 2011 *Phys. Rev. A* **83** 033824
[13] Cheng G L, Zhong W X and Chen A X 2015 *Opt. Express* **23** 9870
[14] Liu Z Z, Chen Y Y, Yuan J Y and Wan R G 2017 *Chin. Phys. B* **26** 124209
[15] Wang L, Zhou F X, Guo H J, Niu Y P and Gong S Q 2016 *Chin. Phys. B* **25** 114205
[16] Bender C M 2007 *Rep. Prog. Phys.* **70** 947
[17] Ganainy R E, Makris K, Christodoulides D and Musslimani Z H 2007 *Opt. Lett.* **32** 2632
[18] Makris K G, Ganainy R E, Christodoulides D and Musslimani Z H 2008 *Phys. Rev. Lett.* **100** 103904
[19] Regensburger A, Bersch C, Miri M A, Onishchukov G, Christodoulides D N and Peschel U 2012 *Nature* **488** 167
[20] Ge L and Türeci H E 2013 *Phys. Rev. A* **88** 053810
[21] Antonosyan D A, Solntsev A S and Sukhorukov A A 2015 *Opt. Lett.* **40** 4575
[22] Peng P, Cao W, Shen C, Qu W, Wen J, Jiang L and Xiao Y 2016 *Nat. Phys.* **12** 1139
[23] Jiang Y, Mei Y, Zuo Y, Zhai Y, Li J, Wen J and Du S 2019 *Phys. Rev. Lett.* **123** 193604
[24] Hang C, Huang G, and Konotop V V 2013 *Phys. Rev. Lett.* **110** 083604
[25] Sheng J, Miri M A, Christodoulides D N and Xiao M 2013 *Phys. Rev. A* **88** 041803
[26] Zhang Z, Zhang Y, Sheng J, Yang L, Miri M A, Christodoulides D N, He B, Zhang Y and Xiao M 2016 *Phys. Rev. Lett.* **117** 123601
[27] Liu Y M, Gao F, Fan C H and Wu J H 2017 *Opt. Lett.* **42** 4283
[28] Shui T, Yang W X, Liu S, Li L and Zhu Z 2018 *Phys. Rev. A* **97** 033819
[29] Tian S C, Wan R G, Wang L J, Shu S L, Lu H Y, Zhang X, Tong C Z, Feng J L, Xiao M and Wang L J 2018 *Opt. Express* **26** 32918
[30] Hang C, Li W and Huang G 2019 *Phys. Rev. A* **100** 043807
[31] Wu J H, Artoni M and Rocca G L 2014 *Phys. Rev. Lett.* **113** 123004
[32] Wu J H, Artoni M and Rocca G L 2015 *Phys. Rev. A* **91** 033811
[33] Wu J H, Artoni M and Rocca G L 2017 *Phys. Rev. A* **95** 053862
[34] Wang X and Wu J H 2016 *Opt. Express* **24** 4289
[35] Yang F, Liu Y C and You L 2017 *Phys. Rev. A* **96** 053845
[36] Jin L 2018 *Phys. Rev. A* **98** 022117
[37] Konotop V V and Zezyulin D A 2018 *Phys. Rev. Lett.* **120** 123902
[38] Ma D, Yu D, Zhao X D and Qian J 2019 *Phys. Rev. A* **99** 033826
[39] Shui T, Yang W X, Li L and Wang X 2019 *Opt. Lett.* **44** 2089
[40] Michler P 2009 *Single Semiconductor Quantum Dots* (Berlin: Springer)
[41] Lodahl P, Mahmoodian S and Stobbe S 2015 *Rev. Mod. Phys.* **87** 347
[42] Li X, Wu Y, Steel D, Gammon D, Stievater T, Katzer D, Park D, Piermarocchi C and Sham L 2003 *Science* **301** 809
[43] Phillips M C, Wang H, Rumyantsev I, Kwong N H, Takayama R and Binder R 2003 *Phys. Rev. Lett.* **91** 183602
[44] Nielsen D and Chuang S L 2010 *Phys. Rev. B* **81** 035305
[45] Muller A, Flagg E B, Bianucci P, Wang X, Deppe D G, Ma W, Zhang J, Salamo G, Xiao M and Shih C K 2007 *Phys. Rev. Lett.* **99** 187402
[46] Abbas M and Qamar S 2020 *Phys. Rev. A* **101** 023821
[47] Villas-Boas J, Govorov A and Ulloa S E 2004 *Phys. Rev. B* **69** 125342
[48] Ramírez H Y and Cheng S J 2010 *Phys. Rev. Lett.* **104** 206402
[49] Krenner H J, Sabathil M, Clark E C, Kress A, Schuh D, Bichler M, Abstreiter G and Finley J J 2005 *Phys. Rev. Lett.* **94** 057402
[50] Müller K, Bechtold A, Ruppert C, Zecherle M, Reithmaier G, Bichler M, Krenner H J, Abstreiter G, Holleitner A W, Villas-Boas J M, Betz M and Finley J J 2012 *Phys. Rev. Lett.* **108** 197402
[51] Ba N, Fei J Y, Li D F, Zhong X, Wang D, Wang L, Wang H H and Bao Q Q 2020 *Chin. Phys. B* **29** 034204
[52] Borges H, Sanz L, Villas-Boas J, Neto O D and Alcalde A 2012 *Phys. Rev. B* **85** 115425
[53] Li Z, Cheng Y, Wei J, Zheng X and Yan Y 2018 *Phys. Rev. B* **98** 115133
[54] Peng Y, Yang A, Chen B, Li L, Liu S and Guo H 2016 *Appl. Phys. Lett.* **109** 141101
[55] Borges H, Alcalde A and Ulloa S E 2014 *Phys. Rev. B* **90** 205311
[56] Mahdavi M, Sabegh Z A, Mohammadi M, Mahmoudi M and Hamedi H R 2020 *Phys. Rev. A* **101** 063811
[57] Kim J, Chuang S L, Ku P C and Chang-Hasnain C J 2004 *J. Phys.: Condens. Matter* **16** S3727
[58] Ortner G, Schwab M, Borri P, Langbein W, Woggon U, Bayer M, Fafard S, Wasilewski Z, Hawrylak P, Lyanda-Geller Y B, Reinecke T L and Forchel A 2004 *Physica E* **25** 249